Noname manuscript No.
(will be inserted by the editor)

Performance metrics of the fixed stress split algorithm for multiphase poromechanics

Saumik Dana · Mohamad Jammoul · Mary F Wheeler

Received: date / Accepted: date

Abstract We focus on the performance of the fixed stress splitting algorithm for the immiscible water-oil flow coupled with linear poromechanics. The two-phase flow equations are solved on general hexahedral elements using the multipoint flux mixed finite element method, whereas, the geomechanics equations are discretized using the conforming Galerkin method. The effects of the coupling parameter on the performance of the fixed stress algorithm is demonstrated for the Frio oil reservoir site.

Keywords Immiscible two phase water-oil flow · poromechanics · coupled system of equations · staggered solution algorithm · mixed finite element method · conforming Galerkin method

1 Introduction

The understanding of the physics of subsurface phenomena is critical to the study of a multitude of applications in the environment and the energy industry such as CO_2 sequestration [1], hydrocarbon extraction [2], water flooding [3] and hydraulic fracturing [4] among many others. This physics is typically governed by the theory of multiphase flow through porous media [5, 6]. The in silico resolution of such physics requires the solution of a complicated set of equations governing the response of the various parameters under the application of thermo-mechanical-hydraulic loading [7–39]. Staggered solution schemes are those in which an operator splitting strategy is used to split the coupled problem into well-posed subproblems which are then solved sequentially instead of solving the coupled system of equations monolithically. The fixed stress split is one such strategy that solves the flow problem while freezing the mean stress followed by the poromechanics problem in repeated iterations until a certain convergence criterion is met at each time step [40–63].
In this paper, we present the fixed stress formulation for the immiscible two-phase (water-oil) flow coupled with linear poromechanics. The fixed stress splitting leads to two updates for the Lagrangian porosity, a fluid update and a mechanics update. The convergence criterion for the fixed stress splitting aims to reduce the difference between the two quantities.
We study the error patterns in the porosity update resulting from adopting a fixed tolerance in the convergence criterion of the splitting algorithm.
This document is structured as follows: the model equations are presented in this Section, the fixed stress split algorithm is presented in Section 2, a numerical result for a field case showing the performance metrics is presented in Section 3 and the conclusions and outlook are presented in Section 4.

Saumik Dana
Mork Family Department of Chemical Engineering and Material Science, University of Southern California, CA 90007

Mohamad Jammoul
Oden Institute for Computational Engineering and Sciences, The University of Texas at Austin, TX 78712

Mary F Wheeler
Oden Institute for Computational Engineering and Sciences, The University of Texas at Austin, TX 78712

1.1 Two-Phase Flow Model

Let $\Omega \subset \mathbb{R}^3$ be the flow domain with boundary $\partial\Omega = \Gamma_D^f \cup \Gamma_N^f$ where Γ_D^f is Dirichlet boundary and Γ_N^f is

Neumann boundary. The equations of flow model are

$$
\begin{aligned}
&\frac{\partial(\phi^* \rho_\beta S_\beta)}{\partial t} + \nabla \cdot \mathbf{z}_\beta - \epsilon \frac{\partial(\phi \rho_\beta S_\beta)}{\partial t} = q_\beta \ (\mathit{mass\ conservation}) \\
&\mathbf{z}_\beta = -\mathbf{K}\lambda_\beta(\nabla p_\beta - \rho_\beta \mathbf{g}) \qquad (\mathit{Darcy's\ law}) \\
&\rho_\beta = \rho_{\beta_0} e^{c_\beta(p_\beta - p_{\beta_0})} \qquad (\mathit{slightly\ compressible\ fluid}) \\
&p_c = p_o - p_w \qquad (\mathit{capillary\ pressure}) \\
&S_w + S_o = 1 \qquad (\mathit{constraint}) \\
&\mathbf{z}_\beta \cdot \mathbf{n} = 0 \text{ on } \Gamma_N^f \times (0,T] \\
&p_\beta(\mathbf{x},0) = p_{\beta_0}(\mathbf{x}),\ \phi(\mathbf{x},0) = \phi_0(\mathbf{x}) \qquad \forall \mathbf{x} \in \Omega
\end{aligned}
$$

where $\beta \equiv w$ for the water (wetting) phase, $\beta \equiv o$ for the oil (non-wetting) phase, $p_\beta : \Omega \times (0,T] \to \mathbb{R}$ are the phase pressures, $\mathbf{z}_\beta : \Omega \times (0,T] \to \mathbb{R}^3$ are the phase fluxes, S_β are the phase saturations, ρ_β are the phase densities, $\phi^* = \phi(1+\epsilon)$ is Lagrangian porosity where ϕ is the Eulerian porosity, and ϵ is the volumetric strain, $\mathbf{n}$ is the unit outward normal on Γ_N^f, q_β is the source or sink term, $\mathbf{K}$ is the uniformly symmetric positive definite absolute permeability tensor, $\lambda_\beta = k_\beta \rho_\beta / \mu_\beta$ are the phase mobilities where k_β are the phase relative permeabilities and μ_β are the phase viscosities, c_β are the fluid compressibilities and $T > 0$ is the time interval. The reader is refered to [64] for an understanding of mixed finite element formulation of flow model.

1.2 Linear Poromechanics Model

Let $\Omega \subset \mathbb{R}^3$ be the poromechanics domain with boundary $\partial\Omega = \Gamma_D^p \cup \Gamma_N^p$ where Γ_D^p is Dirichlet boundary and Γ_N^p is Neumann boundary. The equations are

$$
\begin{aligned}
&\nabla \cdot \boldsymbol{\sigma} + \mathbf{f} = \mathbf{0} \qquad (\mathit{linear\ momentum\ balance}) \\
&\boldsymbol{\sigma} = \mathbb{D}\boldsymbol{\epsilon} - \alpha \bar{p} \mathbf{I} \qquad (\mathit{constitutive\ law}) \\
&\mathbf{f} = \bar{\rho}\phi \mathbf{g} + \rho_r(1-\phi)\mathbf{g} \\
&\bar{p} = p_w S_w + p_o S_o = p_o - p_c S_w \ (\mathit{average\ phase\ pressure}) \\
&\bar{\rho} = \rho_w S_w + \rho_o S_o \qquad (\mathit{average\ phase\ density}) \\
&\boldsymbol{\epsilon}(\mathbf{u}) = \frac{1}{2}(\nabla \mathbf{u} + \nabla^T \mathbf{u}) \qquad (\mathit{small\ strain\ kinematics}) \\
&\mathbf{u} \cdot \mathbf{n}_1 = 0 \text{ on } \Gamma_D^p \times [0,T],\ \boldsymbol{\sigma}^T \mathbf{n}_2 = \mathbf{t} \text{ on } \Gamma_N^p \times [0,T] \\
&\mathbf{u}(\mathbf{x},0) = \mathbf{0} \qquad \forall\ \mathbf{x} \in \Omega
\end{aligned}
$$

where $\mathbf{u} : \Omega \times [0,T] \to \mathbb{R}^3$ is the solid displacement, ρ_r is the rock density, α is the Biot parameter, $\mathbf{f}$ is body force per unit volume, $\mathbf{t}$ is the traction boundary condition, $\boldsymbol{\epsilon}$ is the strain tensor, $\mathbb{D}$ is the fourth order elasticity tensor and $\mathbf{I}$ is the second order identity tensor. The mean stress σ_v is given as

$$
\sigma_v = \frac{1}{3} tr(\boldsymbol{\sigma}) = \frac{1}{3} tr\big(\lambda \epsilon \mathbf{I} + 2G\boldsymbol{\epsilon} - \alpha \bar{p} \mathbf{I}\big)
$$

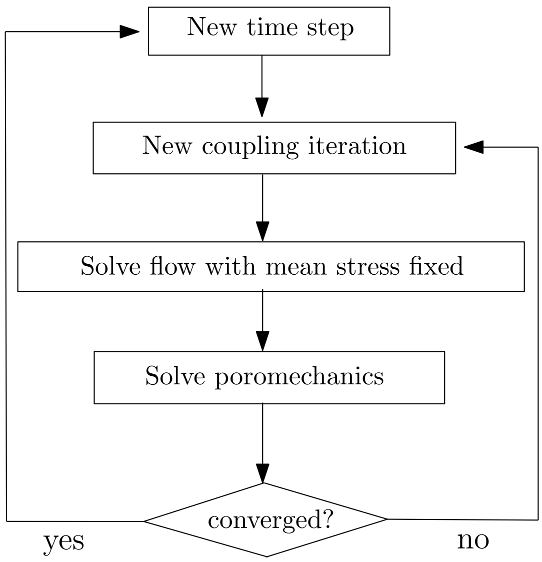

Fig. 1: Flowchart for fixed-stress split iterative scheme for two-phase flow coupled with linear poromechanics.

$$
\begin{aligned}
&= \frac{1}{3} 3\lambda\epsilon + \frac{1}{3} 2G\, \cancel{tr(\boldsymbol{\epsilon})}^{\,\epsilon} - \frac{1}{3} 3\alpha\bar{p} \\
&= \big(\lambda + \frac{1}{3} 2G\big)\epsilon - \alpha\bar{p} = K_b \epsilon - \alpha \bar{p}
\end{aligned}
$$

where K_b is the bulk modulus of the solid skeleton or the drained bulk modulus. The reader is refered to [64] for an understanding of continuous galerkin formulation of poromechanics model.

2 Fixed Stress Split Algorithm

The flowchart of the algorithm is provided in Figure 1. The basic idea of the fixed - stress split strategy is to solve for the pressure and flux degrees of freedom at the current fixed - stress iteration based on the value of the mean stress from the previous fixed - stress iteration. These pressures then contribute to the force vector in the poromechanics system which is solved for displacements thereby updating the stress state. This updated stress state is then fed back to the flow system for the next fixed - stress iteration. The stopping criterion for coupling iterations is designed based on the requirement that the change in Lagrangian porosity during the poromechanics solve in every coupling iteration reduces monotonically from one coupling iteration to the next. Now the change in Lagrangian porosity during the poromechanics solve in any coupling iteration in every time step is given by $\phi^*_{por} - \phi^*_{flow}$ where ϕ^*_{por} is the Lagrangian porosity at the end of the poromechanics solve, ϕ^*_{flow} is the Lagrangian porosity at the end of the flow solve. This quantity is normalized by the current value of Lagrangian porosity as $\frac{\phi^*_{por}-\phi^*_{flow}}{\phi^*_{por}}$ and the stopping criterion is based on the requirement that the maximum norm of this quantity is less than a certain pre-specified tolerance as follows

$$\left\| \frac{\phi^*_{por}-\phi^*_{flow}}{\phi^*_{por}} \right\|_\infty \leq \text{TOL}$$

2.1 Lagrangian Porosity Update During Flow Solve

The nonlinear nature of the equations of two phase flow neccesitate the need for nonlinear iterations in the manner of the Newton-Raphson method. The fixed mean stress constraint is imposed in every Newton iteration. The evolution law for Lagrangian porosity is given by

$$\delta^{(k)}\phi^* = \Psi\delta^{(k)}\bar{p} \tag{2.1}$$

where $\delta^{(k)}(\cdot)$ refers to the change in quantity $(\cdot)$ over the $(k+1)^{th}$ Newton iteration and Ψ is the rock compressibility given by

$$\Psi = \phi\frac{\alpha}{K_b} + (1+\epsilon)\frac{\alpha-\phi}{K_b} \tag{2.2}$$

The reader is refered to [64] for the derivation of (2.1).

2.2 Lagrangian Porosity Update During the Poromechanical Solve

The evolution law for Lagrangian porosity is given by

$$\phi^* = \phi_0 + \alpha\epsilon + \frac{(\alpha-\phi_0)(1-\alpha)}{K_b}(p-p_0) \tag{2.3}$$

The reader is refered to [64] for the derivation of (2.3).

3 Numerical result

In this section, we discuss the numerical results for the Frio oil field site. The simulation was performed using the in-house reservoir simulator IPARS (`https://csm.ices.utexas.edu/IparsWeb/index.html`) on the Bevo3 cluster at the Oden Institute for Computational Engineering and Sciences at the University of Texas at Austin.

3.1 Frio Field Case

The Frio site is an oil field located on the Gulf Coast of the United States near Dayton, Texas. The field has a challenging geometry with several thin faults crossing through. The whole field is curved in the vertical direction with a depth differential of more than 1,000 ft between its parts [65].

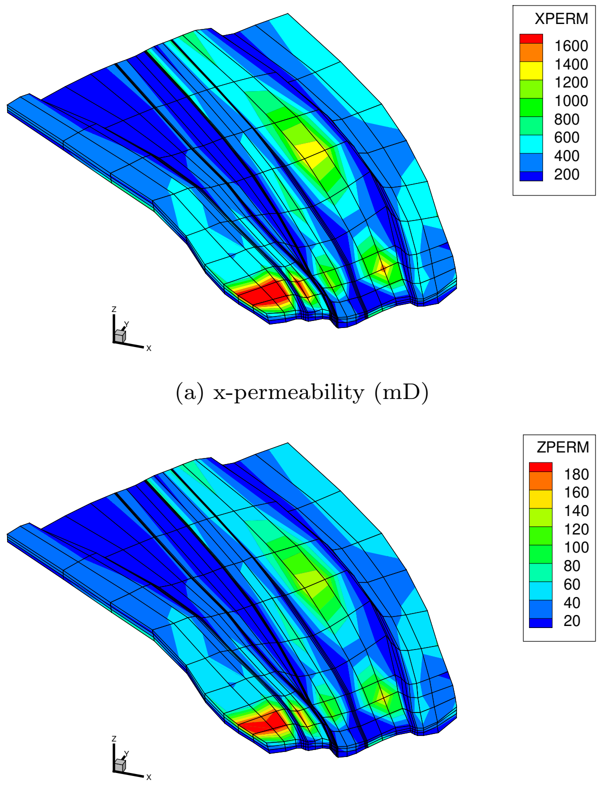

(a) x-permeability (mD)

(b) z-permeability (mD)

Fig. 2: Example 1: Permeability in the x-direction (left) and z-direction (right) for the Frio field.

3.1.1 Configuration and Parameters

We used hexahedral elements to capture the complex reservoir geometry. We have also incorporated the available petrophysical and mechanical information to build a 3D model inside IPARS. Figures 2 show the field geometry and the distribution of the permeability in the x-direction and z-direction relatively.

The computational domain was discretized with $33\times9\times3$ elements. No-flow boundary conditions were imposed for the fluid equations and both stress and displacement boundary conditions were used for the mechanics equations. We assumed a constant porosity $\phi = 0.20$ everywhere in the reservoir. The input parameters for the problem are summarized in Table 1. Three production wells and six injection wells were considered in this example. The locations of the wells are shown in Figures and . All nine wells have constant bottomhole pressure; the values of which are included in Table 1.

Quantity	Value
Time step	$0.05\,days$
Number of grids	$891(33 \times 9 \times 3)$
Absolute permeabilities	$(5.27 \times 10^{-10}\,to\,3.1 \times 10^{3})\,md$
Initial porosity	0.2
Water viscosity	$1.0\,cp$
Oil viscosity	$2.0\,cp$
Initial oil concentration	$44.8\,lbm/ft^3$
Initial oil pressure	$400.0\,psi$
Water compressibility	$1E-6\,psi^{-1}$
Oil compressibility	$1E-4\,psi^{-1}$
Rock density	$165.44\,lbm/ft^3$
Initial water density	$56.0\,lbm/ft^3$
Initial oil density	$62.4\,lbm/ft^3$
Young's Modulus	$1.2E6\,psi$
Poisson's ratio	0.35
Flow boundary conditions	No flow on all boundaries
X+" boundary	$\sigma_{xx} = \sigma \cdot n_x = 10000\,psi$
X-" - boundary	$\mathbf{u} = \mathbf{0}$, zero displacement
Y+" - boundary	$\mathbf{u} = \mathbf{0}$, zero displacement
Y-" - boundary	$\sigma_{yy} = \sigma \cdot n_y = 2000\,psi$
Z+" - boundary	$\mathbf{u} = \mathbf{0}$, zero displacement
Z-" - boundary	$\sigma_{zz} = \sigma \cdot n_z = 1000\,psi$
Injection well (1):	Pressure specified, 4000.0 psi
Injection well (2):	Pressure specified, 3300.0 psi
Injection well (3):	Pressure specified, 4000.0 psi
Injection well (4):	Pressure specified, 4400.0 psi
Injection well (5):	Pressure specified, 3700.0 psi
Injection well (6):	Pressure specified, 4400.0 psi
Production well (1):	Pressure specified, 2000.0 psi
Production well (2):	Pressure specified, 2000.0 psi
Production well (3):	Pressure specified, 2000.0 psi

Table 1: Parameters for the Frio field problem

3.1.2 Results

The initial reservoir state and end of simulation results for the Frio field are displayed in Figures 3 and 4 respectively. The Figures (4a - 4d) show the reference phase pressure, water saturation, oil concentration, and vertical displacement after 60 days. The areas near the wells show significant change in pressure, water saturation, and oil concentration (Figures 4a and 4b). The change in the pressure induced surface subsidence in the uppermost corner of the reservoir as shown in Figure (4d).

We attempt to study the performance of the splitting algorithm by looking at the error at the beginning and end of each fixed stress iteration (Figures 5a and 5b). The error at the first fixed stress iteration of each time step decreases gradually. This can be correlated to the change in pressure in the reservoir. Since all the injection and production wells are pressure specified, the change in the pressure from one time step to another decreases gradually. This leads to a decrease in the error at the start of the fixed stress iteration as long as

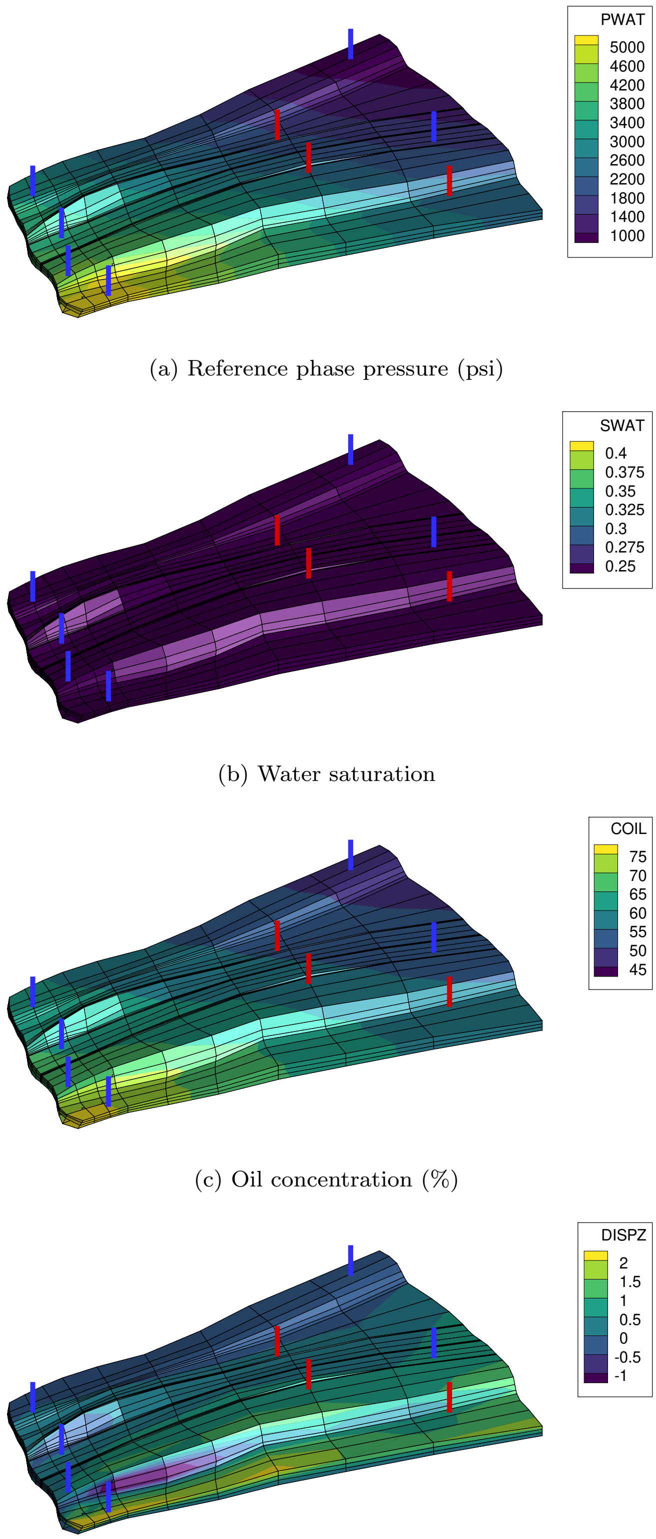

(a) Reference phase pressure (psi)

(b) Water saturation

(c) Oil concentration (%)

(d) Vertical displacements (in)

Fig. 3: Simulation results for the Frio field at time $t = 0.1$ days. The locations of the injection (blue) and production (red) wells are shown.

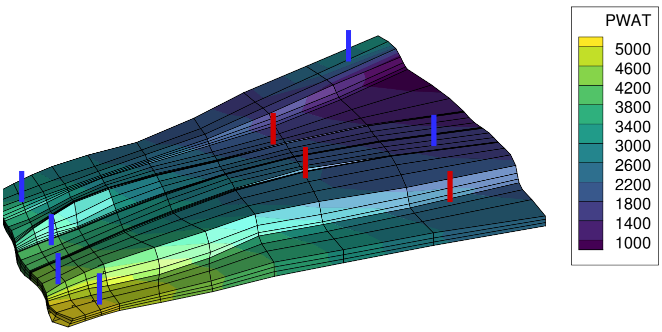

(a) Reference phase pressure (psi)

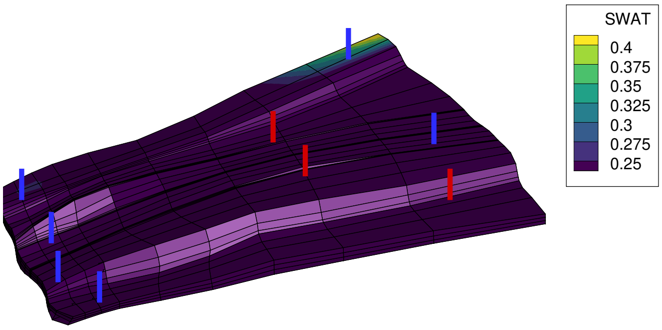

(b) Water saturation

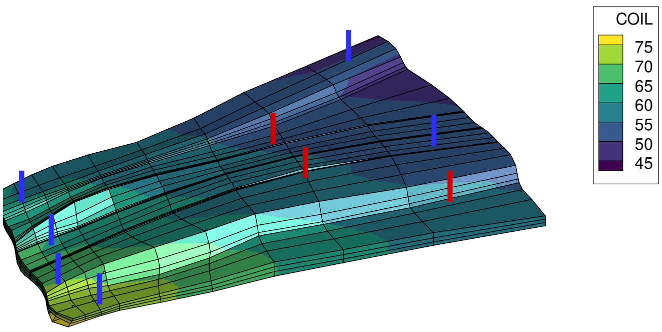

(c) Oil concentration (%)

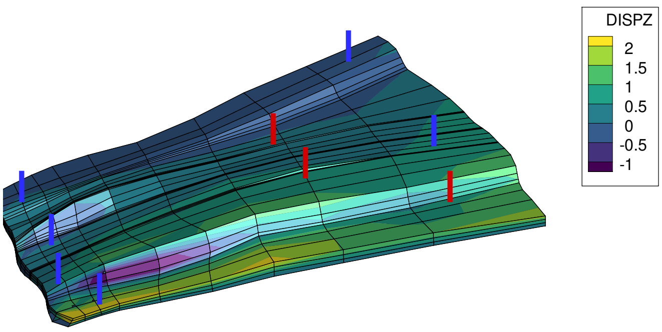

(d) Vertical displacements (in)

Fig. 4: Simulation results for the Frio field at time $t = 60$ days. The locations of the injection (blue) and production (red) wells are shown.

the boundary conditions and source functions of the mechanics equations are independent of time.

The error at the convergence of the fixed stress splitting for each time step is plotted in Figure 5b. The error admits a V-shape cycle and then decreases monotonically afterwards. To understand this behavior, we plot the number of fixed stress iterations for each time step. The increase in error occurred after the number of fixed stress iterations decreased to a single iteration. The error after the first fixed stress iteration, at the 7^{th} time step and onwards, was lower than the $TOL = 10^{-4}$ for all α values, and thus a single iteration was sufficient for the convergence of the algorithm. These observations are consistent with the results of [54] where they reported that using the relative change in mean stress (and equivalently porosity) as a stopping criterion for the fixed-stress iterations may easily lead to over-iteration (or under-iteration), unless the convergence threshold is carefully tuned.

Another aspect to consider is the effect of the coupling parameter, Biot's α, on the performance of the splitting algorithm. By comparing the five plots in Figure 5c, increasing the value of α leads to an increase in the error in the splitting algorithm and to decrease in the computational efficiency. The decrease in computational efficiency can be inferred from the additional fixed stress iterations needed to reach convergence for higher α values. This behavior is expected because the increase in Biot's constant means a stronger coupling between the fluid flow and mechanics. This is evidenced by the fact that the rock compressibility measuring the rate of change of Lagrangian porosity with respect to pore pressure increases with increase in Biot constant as shown in Equation (2.2). This also implies that the porous rock is more sensitive to changes in fluid pressure inside the pores as the Biot constant increases.

4 Conclusions and Outlook

The model equations and algorithmic framework for immiscible two phase flow coupled with linear poromechanics have been presented in this work. We also studied the convergence rates for the fixed stress split method and the impact of the stopping criterion on the performance of the algorithm. The impact of Biot's parameters, namely α, on the convergence and computational efficiency of the fixed stress algorithm was also considered in this work.

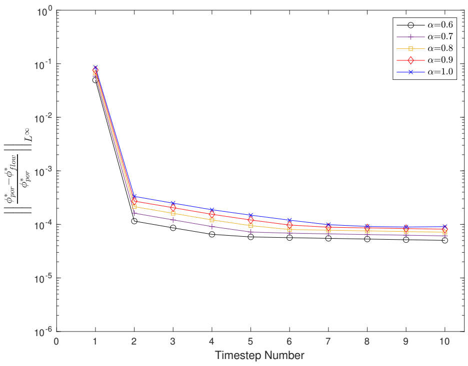

(a) Error after first fixed stress iteration

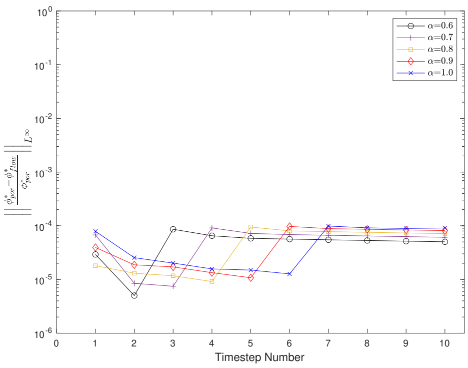

(b) Error after last fixed stress iteration

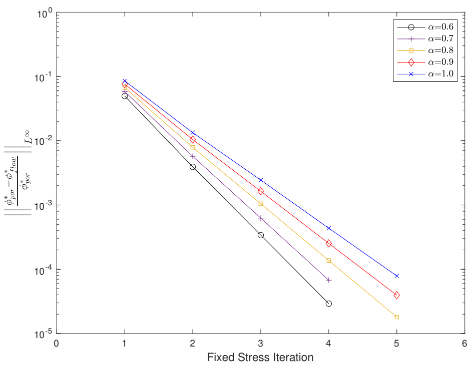

(c) Fixed stress convergence for the first time step

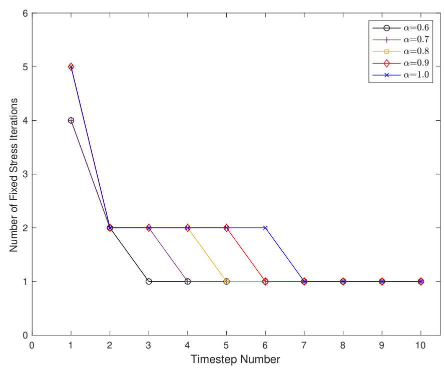

(d) Number of fixed stress iterations

Fig. 5: Fixed stress metrics for the Frio field simulations

Conflict of interest

The authors declare that they have no conflict of interest.

References

1. Thomas Dewers, Peter Eichhubl, Ben Ganis, Steven Gomez, Jason Heath, Mohamad Jammoul, Peter Kobos, Ruijie Liu, Jonathan Major, Ed Matteo, Pania Newell, Alex Rinehart, Steven Sobolik, John Stormont, Mahmoud Reda Taha, Mary Wheeler, and Deandra White. Heterogeneity, pore pressure, and injectate chemistry: Control measures for geologic carbon storage. *International Journal of Greenhouse Gas Control*, 68:203 – 215, 2018.
2. M Jammoul, B Ganis, and MF Wheeler. Effect of reservoir properties on interwell stress interference. In *52nd US Rock Mechanics/Geomechanics Symposium*. American Rock Mechanics Association, 2018.
3. Mohamad Jammoul, Benjamin Ganis, and Mary Wheeler. General semi-structured discretization for flow and geomechanics on diffusive fracture networks. In *SPE Reservoir Simulation Conference*. Society of Petroleum Engineers, 2019.
4. Mohamad Jammoul and Mary F Wheeler. Modeling energized and foam fracturing using the phase field method. Unconventional Resources Technology Conference (URTEC), 2020.
5. R. de Boer. *Theory of Porous Media: Highlights in Historical Development and Current State*. Springer-Verlag Berlin Heidelberg, 1 edition, 2000.
6. O. Coussy. *Poromechanics*. Wiley, 2nd ed edition, 2004.
7. M. R. Correa and M. A. Murad. A new sequential method for three-phase immiscible flow in poroelastic media. *Journal of Computational Physics*, 373:493–532, 2018.
8. Marcos Alcoforado Mendes, Marcio A. Murad, and Felipe Pereira. A new computational strategy for solving two-phase flow in strongly heterogeneous poroelastic media of evolving scales. *International Journal for Numerical and Analytical Methods in Geomechanics*, 36, 2012.
9. Abay Molla Kassa, Sarah Eileen Gasda, Kundan Kumar, and Florin Adrian Radu. Impact of time-dependent wettability alteration on the dynamics of capillary pressure. *Advances in Water Resources*, 142:103631, 2020.
10. Birendra Jha and Ruben Juanes. Coupled modeling of multiphase flow and fault poromechanics during geologic co2 storage. *Energy Procedia*, 63:3313 – 3329, 2014. 12th International Conference on Greenhouse Gas Control Technologies, GHGT-12.
11. Abay M. Kassa, Kundan Kumar, Sarah E. Gasda, and Florin A. Radu. Implicit linearization method for non-standard two-phase flow in porous media, 2019.
12. Florin Adrian Radu, Kundan Kumar, Jan Martin Nordbotten, and Iuliu Sorin Pop. A convergent mass conservative numerical scheme based on mixed finite elements for two-phase flow in porous media, 2015.
13. Florin Adrian Radu, Jan Martin Nordbotten, Iuliu Sorin Pop, and Kundan Kumar. A robust linearization scheme for finite volume based discretizations for simulation of two-phase flow in porous media. *Journal of Computational and Applied Mathematics*, 289:134 – 141, 2015.

14. David Seus, Florin A. Radu, and Christian Rohde. A linear domain decomposition method for two-phase flow in porous media. In Florin Adrian Radu, Kundan Kumar, Inga Berre, Jan Martin Nordbotten, and Iuliu Sorin Pop, editors, *Numerical Mathematics and Advanced Applications ENUMATH 2017*, pages 603–614. Springer International Publishing, 2019.
15. Matteo Cusini, Cor van Kruijsdijk, and Hadi Hajibeygi. Algebraic dynamic multilevel (adm) method for fully implicit simulations of multiphase flow in porous media. *Journal of Computational Physics*, 314:60 – 79, 2016.
16. Jinhyun Choo and Sanghyun Lee. Enriched galerkin finite elements for coupled poromechanics with local mass conservation. *Computer Methods in Applied Mechanics and Engineering*, 341:311 – 332, 2018.
17. Jinhyun Choo, Joshua A White, and Ronaldo I Borja. Hydromechanical modeling of unsaturated flow in double porosity media. *International Journal of Geomechanics*, 16(6):D4016002, 2016.
18. Jinhyun Choo. Large deformation poromechanics with local mass conservation: An enriched galerkin finite element framework. *International Journal for Numerical Methods in Engineering*, 116(1):66–90, 2018.
19. D Jodlbauer, U Langer, and T Wick. Parallel block-preconditioned monolithic solvers for fluid-structure interaction problems. *International Journal for Numerical Methods in Engineering*, 117(6):623–643, 2019.
20. Matteo Cusini, Joshua A. White, Nicola Castelletto, and Randolph R. Settgast. Simulation of coupled multiphase flow and geomechanics in porous media with embedded discrete fractures, 2020.
21. Julia T. Camargo, Joshua A. White, and Ronaldo I. Borja. A macroelement stabilization for mixed finite element/finite volume discretizations of multiphase poromechanics. *Computational Geosciences*, 2020.
22. Matthias A. Cremon, Nicola Castelletto, and Joshua A. White. Multi-stage preconditioners for thermal–compositional–reactive flow in porous media. *Journal of Computational Physics*, 418:109607, 2020.
23. Quan M. Bui, Daniel Osei-Kuffuor, Nicola Castelletto, and Joshua A. White. A scalable multigrid reduction framework for multiphase poromechanics of heterogeneous media. *SIAM Journal on Scientific Computing*, 42:B379–B396, 2020.
24. Joshua A White and Ronaldo I Borja. Block-preconditioned newton–krylov solvers for fully coupled flow and geomechanics. *Computational Geosciences*, 15(4):647, 2011.
25. Joshua A. White, Nicola Castelletto, Sergey Klevtsov, Quan M. Bui, Daniel Osei-Kuffuor, and Hamdi A. Tchelepi. A two-stage preconditioner for multiphase poromechanics in reservoir simulation. *Computer Methods in Applied Mechanics and Engineering*, 357:112575, 2019.
26. Olga Fuks and Hamdi A. Tchelepi. Limitations of physics informed machine learning for nonlinear two-phase transport in porous media. *Journal of Machine Learning for Modeling and Computing*, 1(1):19–37, 2020.
27. Xueying Lu and Mary F. Wheeler. Three-way coupling of multiphase flow and poromechanics in porous media. *Journal of Computational Physics*, 401:109053, 2020.
28. Matteo Frigo, Nicola Castelletto, Massimiliano Ferronato, and Joshua A. White. Efficient solvers for hybridized three-field mixed finite element coupled poromechanics. *Computers & Mathematics with Applications*, 2020.
29. M.D. White, T.J. Kneafsey, Y. Seol, W.F. Waite, S. Uchida, J.S. Lin, E.M. Myshakin, X. Gai, S. Gupta, M.T. Reagan, A.F. Queiruga, S. Kimoto, R.C. Baker, R. Boswell, J. Ciferno, T. Collett, J. Choi, S. Dai, M. De La Fuente, P. Fu, T. Fujii, C.G. Intihar, J. Jang, X. Ju, J. Kang, J.H. Kim, J.T. Kim, S.J. Kim, C. Koh, Y. Konno, K. Kumagai, J.Y. Lee, W.S. Lee, L. Lei, F. Liu, H. Luo, G.J. Moridis, J. Morris, M. Nole, S. Otsuki, M. Sanchez, S. Shang, C. Shin, H.S. Shin, K. Soga, X. Sun, S. Suzuki, N. Tenma, T. Xu, K. Yamamoto, J. Yoneda, C.M. Yonkofski, H.C. Yoon, K. You, Y. Yuan, L. Zerpa, and M. Zyrianova. An international code comparison study on coupled thermal, hydrologic and geomechanical processes of natural gas hydrate-bearing sediments. *Marine and Petroleum Geology*, 120:104566, 2020.
30. Ø. Klemetsdal, A. Moncorgé, O. Moyner, and K. Lie. Additive schwarz preconditioned exact newton method as a nonlinear preconditioner for multiphase porous media flow. 2020(1):1–20, 2020.
31. A. Møyner, O.; Moncorgé. Nonlinear domain decomposition scheme for sequential fully implicit formulation of compositional multiphase flow. *Computational Geosciences*, 2019.
32. Gaute Linga, Olav Møyner, Halvor Møll Nilsen, Arthur Moncorgé, and Knut-Andreas Lie. An implicit local timestepping method based on cell reordering for multiphase flow in porous media. *Journal of Computational Physics: X*, 6:100051, 2020.
33. Hadi Hajibeygi, Manuela Bastidas Olivares, Mousa HosseiniMehr, Sorin Pop, and Mary Wheeler. A benchmark study of the multiscale and homogenization methods for fully implicit multiphase flow simulations. *Advances in Water Resources*, 143:103674, 2020.
34. Ludovica Delpopolo Carciopolo, Luca Formaggia, Anna Scotti, and Hadi Hajibeygi. Conservative multirate multiscale simulation of multiphase flow in heterogeneous porous media. *Journal of Computational Physics*, 404:109134, 2020.
35. El-Amin, Mohamed F., Kou, Jisheng, and Sun, Shuyu. Theoretical stability analysis of mixed finite element model of shale-gas flow with geomechanical effect. *Oil Gas Sci. Technol. - Rev. IFP Energies nouvelles*, 75:33, 2020.
36. Jihoon Kim, I.Yucel Akkutlu, Tim Kneafsey, Joo Yong Lee, George J. Moridis, Jeremy Adams, Tae Woong Ahn, Sharon Borglin, Bin Wang, Hyun Chul Yoon, Sangcheol Yoon, Xuyang Guo, John Killough, and Peng Zhou. Advanced simulation and experiments of strongly coupled geomechanics and flow for gas hydrate deposits: Validation and field application. 3 2020.
37. Yidong Zhao and Jinhyun Choo. Stabilized material point methods for coupled large deformation and fluid flow in porous materials. *Computer Methods in Applied Mechanics and Engineering*, 362:112742, 2020.
38. TT Garipov, P Tomin, R Rin, DV Voskov, and HA Tchelepi. Unified thermo-compositional-mechanical framework for reservoir simulation. *Computational Geosciences*, 22(4):1039–1057, 2018.
39. T. Kadeethum, S. Lee, F. Ballarind, J. Choo, and H.M. Nick. A locally conservative mixed finite element framework for coupled hydro-mechanical-chemical processes in heterogeneous porous media, 2020.
40. J. Kim, H. A. Tchelepi, and R. Juanes. Stability, accuracy and efficiency of sequential methods for coupled flow and geomechanics. *SPE Journal*, 16(2):249–262, 2011.

41. A. Mikelić and M. F. Wheeler. Convergence of iterative coupling for coupled flow and geomechanics. *Computational Geosciences*, 17(3):455–461, 2013.
42. Andro Mikelić, Bin Wang, and Mary F. Wheeler. Numerical convergence study of iterative coupling for coupled flow and geomechanics. *Computational Geosciences*, 18:325–341, 2014.
43. N. Castelletto, J. A. White, and H. A. Tchelepi. Accuracy and convergence properties of the fixed-stress iterative solution of two-way coupled poromechanics. *International Journal for Numerical and Analytical Methods in Geomechanics*, 39(14):1593–1618, 2015.
44. T. Almani, K. Kumar, A. Dogru, G. Singh, and M. F. Wheeler. Convergence analysis of multirate fixed-stress split iterative schemes for coupling flow with geomechanics. *Computer Methods in Applied Mechanics and Engineering*, 311:180–207, 2016.
45. T. Almani, K. Kumar, and M. F. Wheeler. Convergence and error analysis of fully discrete iterative coupling schemes for coupling flow with geomechanics. *Computational Geosciences*, 2017.
46. J. W. Both, M. Borregales, J. M. Nordbotten, K. Kumar, and F. A. Radu. Robust fixed stress splitting for biot's equations in heterogeneous media. *Applied Mathematics Letters*, 68:101–108, 2017.
47. Elyes Ahmed, Jan Martin Nordbotten, and Florin Adrian Radu. Adaptive asynchronous time-stepping, stopping criteria, and a posteriori error estimates for fixed-stress iterative schemes for coupled poromechanics problems. *Journal of Computational and Applied Mathematics*, 364:112312, 2020.
48. Erlend Storvik, Jakub Wiktor Both, Jan Martin Nordbotten, and Florin Adrian Radu. The fixed-stress splitting scheme for biot's equations as a modified richardson iteration: Implications for optimal convergence, 2019.
49. Jakub Wiktor Both, Kundan Kumar, Jan Martin Nordbotten, and Florin Adrian Radu. Anderson accelerated fixed-stress splitting schemes for consolidation of unsaturated porous media. *Computers and Mathematics with Applications*, 77(6):1479 – 1502, 2019. 7th International Conference on Advanced Computational Methods in Engineering (ACOMEN 2017).
50. Manuel Borregales, Kundan Kumar, Florin Adrian Radu, Carmen Rodrigo, and Francisco José Gaspar. A partially parallel-in-time fixed-stress splitting method for biot's consolidation model. *Computers and Mathematics with Applications*, 77(6):1466 – 1478, 2019. 7th International Conference on Advanced Computational Methods in Engineering (ACOMEN 2017).
51. Andrea Franceschini, Nicola Castelletto, and Massimiliano Ferronato. Block preconditioning for fault/fracture mechanics saddle-point problems. *Computer Methods in Applied Mechanics and Engineering*, 344:376 – 401, 2019.
52. Massimiliano Ferronato, Andrea Franceschini, Carlo Janna, Nicola Castelletto, and Hamdi A. Tchelepi. A general preconditioning framework for coupled multiphysics problems with application to contact- and poro-mechanics. *Journal of Computational Physics*, 398:108887, 2019.
53. Manuel Antonio Borregales Reverón, Kundan Kumar, Jan Martin Nordbotten, and Florin Adrian Radu. Iterative solvers for biot model under small and large deformations. *Computational Geosciences*, pages 1–13, 2020.
54. Vivette Girault, Xueying Lu, and Mary F. Wheeler. A posteriori error estimates for biot system using enriched galerkin for flow. *Computer Methods in Applied Mechanics and Engineering*, 369:113185, 2020.
55. Saumik Dana, Benjamin Ganis, and Mary F. Wheeler. A multiscale fixed stress split iterative scheme for coupled flow and poromechanics in deep subsurface reservoirs. *Journal of Computational Physics*, 352:1–22, 2018.
56. Saumik Dana and Mary F Wheeler. Design of convergence criterion for fixed stress split iterative scheme for small strain anisotropic poroelastoplasticity coupled with single phase flow. *arXiv preprint arXiv:1912.06476*, 2019.
57. Saumik Dana. System of equations and staggered solution algorithm for immiscible two-phase flow coupled with linear poromechanics. *arXiv preprint arXiv:1912.04703*, 2019.
58. Saumik Dana, Joel Ita, and Mary F Wheeler. The correspondence between voigt and reuss bounds and the decoupling constraint in a two-grid staggered algorithm for consolidation in heterogeneous porous media. *Multiscale Modeling & Simulation*, 18(1):221–239, 2020.
59. Saumik Dana, Joel Ita, and Mary F Wheeler. The correspondence between voigt and reuss bounds and the decoupling constraint in a two-grid staggered algorithm for consolidation in heterogeneous porous media. *Multiscale Modeling & Simulation*, 18(1):221–239, 2020.
60. Saumik Dana, Xiaoxi Zhao, and Birendra Jha. Two-grid method on unstructured tetrahedra: Applying computational geometry to staggered solution of coupled flow and mechanics problems. *arXiv preprint arXiv:2102.04455*, 2021.
61. S. Dana and M. F. Wheeler. Convergence analysis of fixed stress split iterative scheme for anisotropic poroelasticity with tensor biot parameter. *Computational Geosciences*, 22(5):1219–1230, 2018.
62. S. Dana and M. F. Wheeler. Convergence analysis of two-grid fixed stress split iterative scheme for coupled flow and deformation in heterogeneous poroelastic media. *Computer Methods in Applied Mechanics and Engineering*, 341:788–806, 2018.
63. S. Dana. *Addressing challenges in modeling of coupled flow and poromechanics in deep subsurface reservoirs.* PhD thesis, The University of Texas at Austin, 2018.
64. S. Dana. *Addressing challenges in modeling of coupled flow and poromechanics in deep subsurface reservoirs.* PhD thesis, The University of Texas at Austin, 2018.
65. M. Juntunen and M. F. Wheeler. Two-phase flow in complicated geometries. *Computational Geosciences*, 17(2):239–247, 04 2013.